Chapter

Plasma Resistance Evaluation and Characteristics of Yttria Ceramics Sintered by Using Calcination Yttria

Jin Sam Choi

Abstract

The evaluation of plasma resistance and the characteristics of yttria ceramics fabricated by calcination yttria as a starting material without dopants under an oxidation atmosphere were investigated. Regardless of the starting materials, as-received and calcined yttria powder, XRD patterns showed that all samples have Y_2O_3 phase. The three cycling processes inhibited a large grain, which occurs frequently during the yttria sintering, and a high-density ceramic with a homogeneous grain size was obtained. The smaller the grain size, the larger were the Young's modulus and K_{IC}. Compared to Al_2O_3 and ZrO_2 ceramics, yttria ceramics showed 3 times larger plasma resistance and 1.4–2.2 times lower weight loss during the plasma etching test, respectively. The characteristics of pure hot-pressed yttria ceramics tempered in an oxidation atmosphere are also investigated. Even though the color variation of the hot-pressed Y_2O_3 ceramics was due to the sintering temperatures, the oxidation process turned the color of the Y_2O_3 ceramics into white. In addition, oxygen defects also affected the weight change and microstructure of the Y_2O_3 ceramics. The Y_2O_3 ceramic sintered at 1600°C had obtained a full density. As the sintering temperature increased, small homogeneous grains grew to large grains which affected the Vickers hardness.

Keywords: as-received yttria, calcined yttria, three-repeated cycle sintering, homogeneous grain, plasma resistance, hot-pressed yttria ceramics, oxidation, homogeneous grain, full density

1. Approach to sintering a yttria monolith to full density by surface and interfacial engineering

1.1 Introduction

Yttria, Y_2O_3, has great potential as a host material for solid-state lasers such as yttrium aluminum garnet-doped neodymium, Nd:YAG, and yttrium oxide doped with ytterbium, Yb:Y_2O_3 [1, 2]. Other commonly known oxides, such as Al_2O_3, MgO, and ZrO_2 ceramics, have attracted more interest than yttria [3, 4]. Therefore, the application of yttria ceramics in modern industry has been limited. Yttria ceramics are strongly dependent on not only their intrinsic properties but also their crystal structure. Yttria, which has a C-type rare earth sesquioxide structure, needs

to be derived from the cubic fluorite-type structure by removing one quarter of the oxygen atoms [5]. Yttria has 32 yttrium and 48 oxygen ion sites per unit cell. This structure has large interstitial sites with the same size as an oxygen ion in the anion sublattice. Yttria has a cubic or alpha-type crystal structure until the temperature reaches 2325°C. The phase transition to a tetragonal crystal structure also occurs at 2325°C. A stable phase, known as hexagonal or beta-type, is maintained until it reaches the melting temperature, 2340°C [6].

Recently, yttria, which is used widely in partially stabilized zirconia and sintering aids, was the center of attention in the semiconductor industry because yttria is superior to quartz, Al_2O_3, ZrO_2, BN, and SiC in terms of its radical or cationic resistance activated by plasma [7] and sintering-limiting property [6].

Nevertheless, when the synthesis of nanoparticles using coprecipitation was carried out and the influence of precursors or additives was examined, it was reported that yttria, sintered under vacuum or hydrogen conditions, was close to the theoretical density [8–10]. The additives affected the grain boundary migration. This compensated for the charge, cation diffusion, solute transport, and additive-defect interaction [11, 12]. According to Huang et al. [13], the theoretical density of yttria ceramic was obtained by the two-step sintering and vacuum sintering of a lanthanum-doped yttria ceramic combination. Previous studies [14–16] attempted to improve the yttria transmittance and electrical conduction of the body sintered using special techniques, such as spark plasma sintering, microwave-flash combustion synthesis, hot isostatic pressing, and the addition of tri- or tetravalent additives. Therefore, it is necessary to examine the intrinsic sintering characteristics of yttria itself. More recently, Choi et al. [17] reported not only the behavior, color, and density of yttria ceramics but also the weight change due to oxygen vacancies and oxygen diffusion in a sintered body as a function of the sintering temperature. They suggested that the changes in color, density, weight, and microstructure of grains according to the sintering temperature were related to the volatilization of yttrium ions at oxygen vacancies in the lattice site at high temperatures [8, 10, 11]. On the other hand, the sintering property of the starting material, calcined yttria, from which the hydration reaction had been eliminated, as expressed in Eq. (1), but oxygen diffusion in oxygen vacancies and yttria powder, which removes gas spouting of the precursor, occurred continuously up to 1250°C, is unknown [13, 15]:

$$RE\,(H_2O)_n^{3+} + H_2O \left[RE(OH)\,(H_2O)_n^{-1}\right]^{2+} + H_3O^+ \qquad (1)$$

where *RE* and $_n$ represent the coordination number of rare earth and cation, respectively.

To determine the effects of oxygen vacancies and hydration on the sintering properties of yttria, this study studied the sintering characteristics of yttria calcined without a gas or hydration reaction containing a hydration reagent of precursors. In addition, when oxygen diffusion occurred in the oxygen vacancies, the yttria powder was heated repeatedly to adopt the result of density and increasing weight. The plasma resistivity of the yttria ceramic was compared with that of the control group.

1.2 Y_2O_3 as a host material and fabrication methods for the potential applications

1.2.1 Y_2O_3 structure and dopant

Y_2O_3 has a C-type cubic structure of rare earth oxides. The C-type structure is due to the bixbyite (space group Ia3 (Th7) with X = 16) and is similar to the fluorite

(CaF_2)-type structure, in which there is a quarter of empty anion sites and they are arranged regularly (**Figure 1**).

Three quarters of the cations are in cubes, in which the missing oxygen ions are along the face diagonal. One quarter of the cations are in cubes, in which the missing oxygen ions are along the body diagonal. The unit cell contains 48 oxygen and 32 yttrium ions. Yttrium ions are located at the center of an approximate cube, and oxygen ions are located at six of the eight vertices [1, 18]. In three quarters of these sites, the missing oxygen ions are located on a face diagonal of the mini-cube, and the rest are located at the ends of a body diagonal. The full unit cell contained 4 × 4 × 4 of these mini-cubes. Here, only a 2 × 2 × 1 part is shown for clarity of presentation. As an oxide, yttria showed broad transmittivity from 280 nm to 8 μm. Y_2O_3 melts at 2430°C, but the C-type structure was only stable up to 2325°C [6]. The H-type structure has a hexagonal form at high temperatures. The high melting temperature and this polymorphic transition make the growth of yttria single crystals difficult. Like fluorite-structured oxides, oxygen vacancies and interstitials are the major defects in pure yttrium oxide [19].

In fluorite-structured oxides, Y_2O_3 can dissolve a large amount of aliovalent cations. This is accompanied by the formation of charge-compensation oxygen vacancies when accepted dopants are present and donor dopants are present in the oxygen interstitials. These anion defects facilitate oxygen diffusion. Indeed, oxygen anion diffusion was much faster than yttrium cation diffusion in pure Y_2O_3. Therefore, cation diffusion is the rate control step for grain boundary migration at all compositions. Because cation doping can be conducted readily within the solubility limit, Y_2O_3 like CeO is a good candidate for examining the cation dopant effects on grain boundary mobility [18]. The cubic symmetry of this oxide further ensured a lack of strong anisotropy in grain boundary mobility, which could otherwise complicate grain growth behavior.

Dopants of both donor and acceptor types as additives for sintering yttria at lower temperatures include Mg^{2+}, Sr^{2+}, Sc^{3+},Yb^{3+}, Gd^{2+}, La^{3+}, Ti^{4+}, Zr^{4+}, Ce^{4+}, and Nb^{5+} [19, 20]. The role of the dopant in yttria is similar to fluorite-structured oxide estimated from several important features. The grain boundary mobility by cation diffusion involves an interstitial mechanism. Solute drag could suppress grain boundary mobility at high dopant concentrations. Grain boundary mobility is influenced by a dopant-defect interaction, which is charge and size dependent. Moreover, undersized dopants have a tendency to enhance grain boundary mobility markedly due to distortion of the surrounding lattice that apparently facilitates

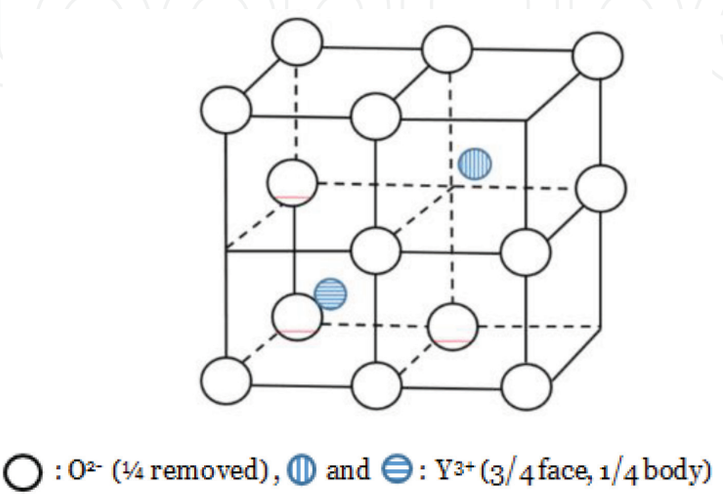

Figure 1.
Crystal structure of Y_2O_3.

defect migration [12, 18]. According to Kingery et al. [21], the diffusion of oxygen anions in yttria is much faster than that of yttrium cations. Hence, yttrium cation interstitial diffusion is the rate control step for grain boundary migration.

1.2.2 Yttria ceramic fabrication

Yttria has potential applications, such as missile domes and bulb envelopes because of its optical transparency and a host material for solid-state lasers and high-resistance materials for etching plasma. Several studies have focused on obtaining full-density or high-transparency polycrystalline yttria ceramics. In the former, several methods have attempted to control the particle size and its distribution, coprecipitation, dopants or additives, and homogeneity, through hydrothermal methods. In the latter, a novel sintering method was studied. A combination of vacuum sintering and hot isostatic pressing methods was based on the low-temperature sintering process to suppress grain growth without sacrificing densification. The pores can be removed completely after hot isostatic pressing. These results are based on the addition of additives in yttria. Ikegami et al. [22] reported the fabrication of transparent ceramics by the two-temperature sintering of yttrium hydroxide with near theoretical total transmittance. Haung et al. [13] synthesized lanthanum-doped yttria ceramic by a combination of two-step sintering and vacuum sintering. A two-step strategy was proposed to produce materials with near theoretical total transmittance, and these studies focused on transparent ceramics used as infrared windows.

1.3 Sample fabrication

The sample preparation was as follows. Yttria powder (99.9%, UUHP, Shin-Etsu Chemical Co. Ltd., Japan) was used as the starting material of as-received yttria. ASY and CY powder was prepared by calcination at 1250°C for 48 h. The powder of fused yttria, FY (Mirae Materials Co. Korea), by induction melting was ball milled with 300 μm zirconia ball media for 24 h. After milling, the powder mixtures were dried at 500°C for 24 h and sieved with 325 mesh to achieve uniform particle sizes. Here, the graphite mold having a diameter of 60 mm was filled with 100 g of the starting material. After forming one axis at 200 kg, cold isostatic pressing (CIP) was performed at a 300 bar pressure to increase the green density. The heating and cooling rates were 5°C/min. The sintered specimens listed in **Table 1** were obtained by the thermal history shown in **Figure 2**.

In the crystal phase, a coarse grain microstructure, and a microstructure of specimen, the specimens were observed using X-ray diffraction (XRD, D/MAX-2550V, Rigaku, Japan), polarizing microscope (Eclipse LV100, Nikon, Japan), and scanning electron microscope (SEM, JSM-6700F, Jeol, Japan), respectively, while bulk density of the sintered specimens was measured according to the ASTM D6683-14 method. The modulus of elasticity of the sintered specimens was observed using a pulse echo device (5800 Pulser/Receiver, Panametrics, Japan) with an oscilloscope (Tektronix, TDS3012, Japan) of X- and Y-modulation, longitudinal, and transverse waves. K_{IC} (HV-100, Mitutoyo, Japan) was measured by applying a load of 500 g on average of 10 times or more after the specimen surface was polished with 0.2 μm diamond paste. The etching depth and the weight reduction rate were obtained by surface roughness (Surfcorder ET3000, Kosaka Lab., Japan) after plasma etching for 60 min by using an inductively coupled plasma system (Versiline, UNAXIS Co., USA). Sintering properties and plasma evaluation were compared with yttria ceramics sintered, Al_2O_3 (99.6%, Semiconductor Wafer, Inc., Taiwan), ZrO_2 (Semiconductor Wafer, Inc., Taiwan), Si wafer (Sumco Co., Japan), and quartz (General Electric (GE), USA), respectively.

Name	Starting materials
ASY	As-received yttria
CY	Calcined yttria, at 1250°C for 24 h in air
FY	Fused yttria by induction melting
HY [17]	Hot-pressed, at 1600°C for 8 h under Ar gas

Table 1.
Yttria ceramics named and prepared.

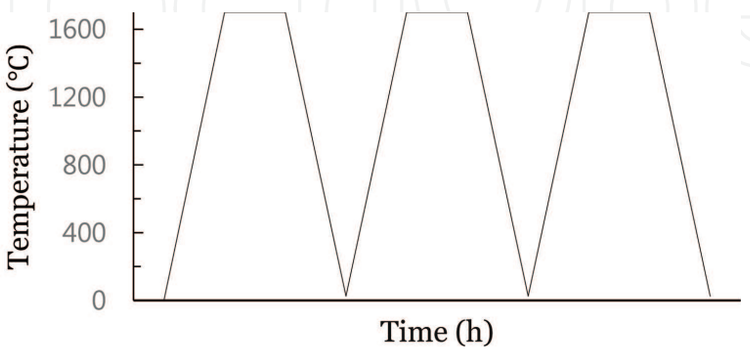

Figure 2.
Sintering schedule of the three-repeated cycle in air.

1.4 Characteristic evaluation of yttria ceramics sintered by three-repeated cycle

Table 1 lists the names of yttria ceramic specimens. **Figure 3** shows the XRD crystal phase of the yttria ceramic sintered under the conditions in **Figure 2**. X-ray diffraction analysis (XRD, D/MAX-2550V, Rigaku, Japan) was conducted to determine the crystal structure of the prepared yttria ceramics sintered using CuKα1 radiation between 5 and 70° (2θ) at room temperature. The crystal phase of CY, the calcined starting material, was identified as Y_2O_3, but ASY contained both Y_2O_3 and $YO_{1.335}$.

The difference in the crystallographic phase depending on the starting material is believed to be the effect of the oxygen vacancies, which was about one-fourth of the 48 standard positions [5, 11, 15].

The starting material calcined at 1250°C for 48 h was exposed to hydration and precursor gases, whereas ASY exhibited continuous volatilization of precursors up to 1250°C [10, 16]. Rhodes et al. [23] examined the continuous volatilization of methane gas. They observed not only the release of carbon or water impurities but also carbonization and hydration reactions until the temperature reached 1200°C. At higher temperatures, the calcined starting material was found to be free from the influence of the adsorption gas and hydration reaction of the precursor [5, 9, 10, 16]. A mixture phase of Y_2O_3 and $YO_{1.335}$ in ASY was obtained after the sintering, and the relative oxygen filling was less than CY [13]. Based on this, similar study results were reported; the self-diffusion coefficient and activation energy at 1050–1250°C were 6×10^{-6} cm^2/s and 82 kJ/mole, respectively [24]. Swamy et al. [25] suggested the possibility of a fluorite crystal phase formation due to the irregular oxygen vacancies in the unit lattice according to high-temperature XRD equipment.

In addition, there was a difference between the results in that the additive affected only the change in transmittance, $YO_{1.401}$ or $YO_{1.335}$ phase formation, and the crystalline phase of the monoclinic were mixed depending on the heat treatment conditions. On the other hand, these results are common in that it originated from oxygen vacancies in

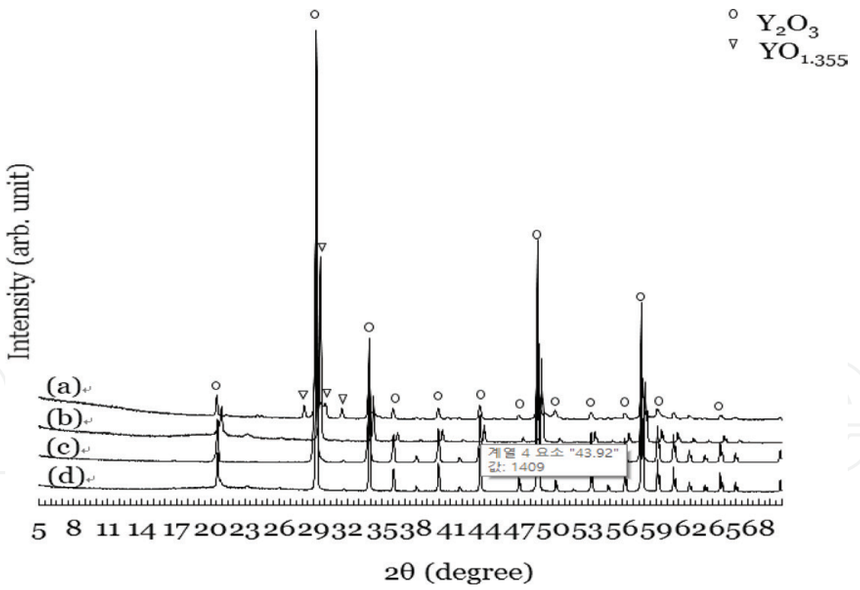

Figure 3.
XRD patterns of yttria ceramics sintered. (a) ASY, as-received yttria; (b) CY, calcined yttria; (c) FY, fused yttria; and (d) HY [17], hot-pressed yttria.

the yttria regular site [13, 18, 24]. The density of the CY specimen was 4.9 g/cm^3, which is higher than that of ASY, 4.8 g/cm^3, as shown in **Figure 4**. On the other hand, CY, calcined yttria, and ASY, repeated-cycle sintering yttria, corresponding to the density of commercial yttria (Y0100A, Kyocera, Japan) and 4.9 g/cm^3 were effective sintering methods, despite being lower than the theoretical density (5.01 g/cm^3) of the HY specimen.

Figure 5 shows a coarse grain microstructure of the CY specimen, in which the surface of the specimen was polished with a 0.2 μm diamond paste, regardless of the starting material condition. The microstructure after repeated-cycle sintering revealed a large number of open pores, in which the hydration reactant and precursor gas of formula (1) were observed, but no coarse particles were observed in the ASY specimen in **Figure 6(a)** [9, 24].

In addition, the CY specimen showed a relatively dense microstructure, as shown in **Figure 6(b)**. The coarse particles in the initial stage changed to uniform particles after repeat-cycle sintering of yttria in air (see **Figures 5** and **6(a)**). Because Y_2O_3 is an oxygen-deficient complex, it is easy to deviate from the stoichiometric Y:O ratio of 40:60 (at.%) due to oxygen vacancies [13, 25]. The majority

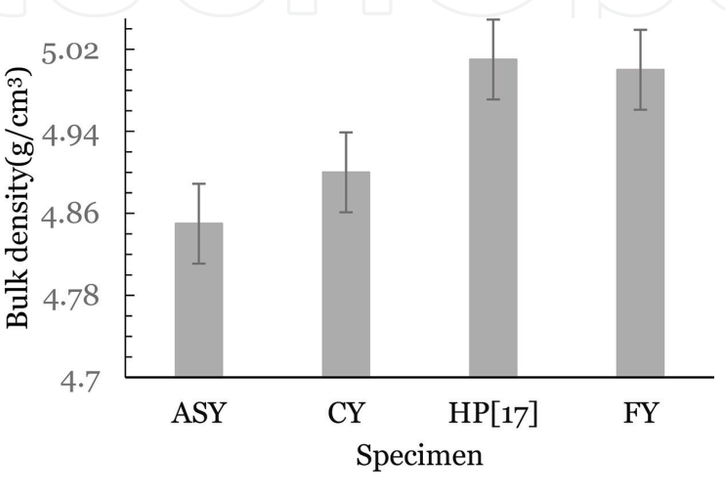

Figure 4.
Bulk density of yttria ceramics sintered.

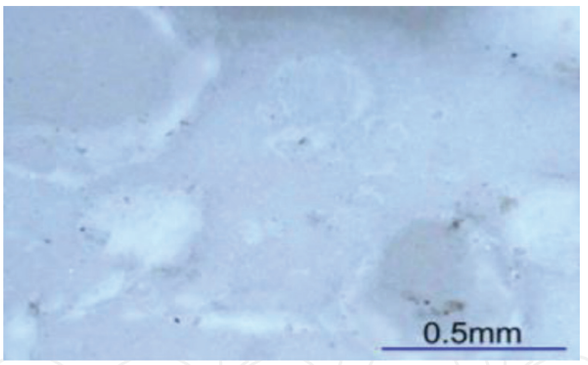

Figure 5.
Optical photograph of the polished surface of CY, yttria ceramics, the first step sintered at 1700°C for 6 h in air. Different granules in the matrix represent abnormal grain growth. The black dots show the remaining polishing powders.

phase of $YO_{1.335}$ with oxygen deficiencies appeared in only the ASY specimen observed in XRD patterns in **Figure 3**.

A thermodynamically stable liquid phase formed locally at 1522°C when the Y:O ratio was 60:40 (at.%), which resulted in pyrolysis of the liquid phase in the repeated heat treatment [25]. The reasons why the rough particles of **Figure 5**, which appeared at the initial stages of less-pressure sintering of yttria, changed to homogeneous particles like the microstructure in **Figure 6(a)** after repeated sintering are as follows. As Y_2O_3 is an oxygen-deficient body, it is easy to deviate from the stoichiometric Y:O ratio range of 40:60 (at.%) due to oxygen vacancies [13]. In **Figure 3(a)**, which showed the XRD crystal phase, only the $YO_{1.335}$ crystal phase with oxygen deficiencies appeared in the ASY specimen. The liquid phase was thermodynamically stable, formed locally at 1522°C and decomposed thermally in the repeated heat treatment, resulting in a crystal when the Y:O ratio was in 60:40 (at.%). The coarse particles in **Figure 5** were prepared by the liquid phase formation when the Y:O ratio was 60:40 (at.%) at 1522°C.

This liquid phase changed stoichiometrically at a Y:O ratio of 40:60 (at.%) due to oxygen diffusion in the lattice during repeated sintering. Therefore, the coarse particles in **Figure 4** disappear because it could change into a crystalline phase rather than exist in the liquid phase [25, 26]. **Figure 7** shows the Y-O phase diagram at 1522°C when the Y:O ratio was 60:40 (at.%); coarse particles support the validity of liquid phase formation hypothesis. This liquid phase changed stoichiometrically at a Y:O ratio (at.%) of 40:60 due to oxygen diffusion in the lattice during the repeated

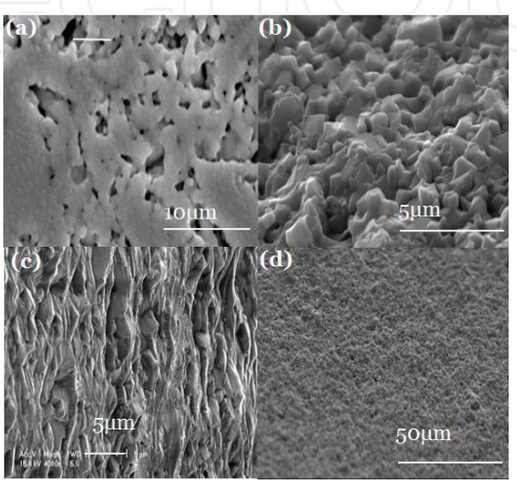

Figure 6.
SEM images of (a) ASY, as-purchased Y_2O_3 powder; (b) CY, calcined Y_2O_3 powder at 1250°C for 48 h in air; (c) fused yttria by induction melting; and (d) HY, hot-pressed yttria [17].

sintering. Therefore, it is believed that the coarse particles shown in **Figure 4** disappear because the crystalline phase was more stable than the liquid phase, but this hypothesis will be proven through further studies. **Figure 8(a)** and **(b)** showed the Vickers indentation results of the ASY and CY specimens. Stress propagation along the cleavage plane and the low-level mist shape were distinct from the HY specimen, which was similar to the glass-like microstructure in **Figure 8(c)**.

The Young's modulus increased with decreasing particle size, as listed in **Table 2**, where average values of the indentation of the specimens, K_{IC}, were measured to apply a 500 g load more than ten times. On the other hand, the HY specimen K_{IC} appeared to be relatively high regardless of the particle size because the dense microstructure, crystal phase, and the amorphous phase were mixed as shown in **Figures 6(c)** and **8(c)** [26, 27]. **Figure 9** presents the plasma resistivity profiles of the sintered specimens and the control group. From Eqs. (2) and (3), the etching depth and weight reduction rate were obtained by surface roughness after plasma etching for 60 min using an inductively coupled plasma system by masking the abrasive specimen.

The sintering properties and plasma evaluation of yttria ceramic were compared with Al_2O_3 (Semiconductor Wafer, Inc., Taiwan), ZrO_2 (Semiconductor Wafer, Inc., Taiwan), Si wafer (Sumco Co., Japan), and quartz (General Electric) [11]. The etch rate and weight loss rate, which are related directly to the plasma resistance, were calculated as follows. The evaluation of plasma etching was performed using simple equations:

$$\text{Etch rate } (\mu\text{m min}) = \text{etch depth } (\mu\text{m})/\text{exposure time (min)} \quad (2)$$

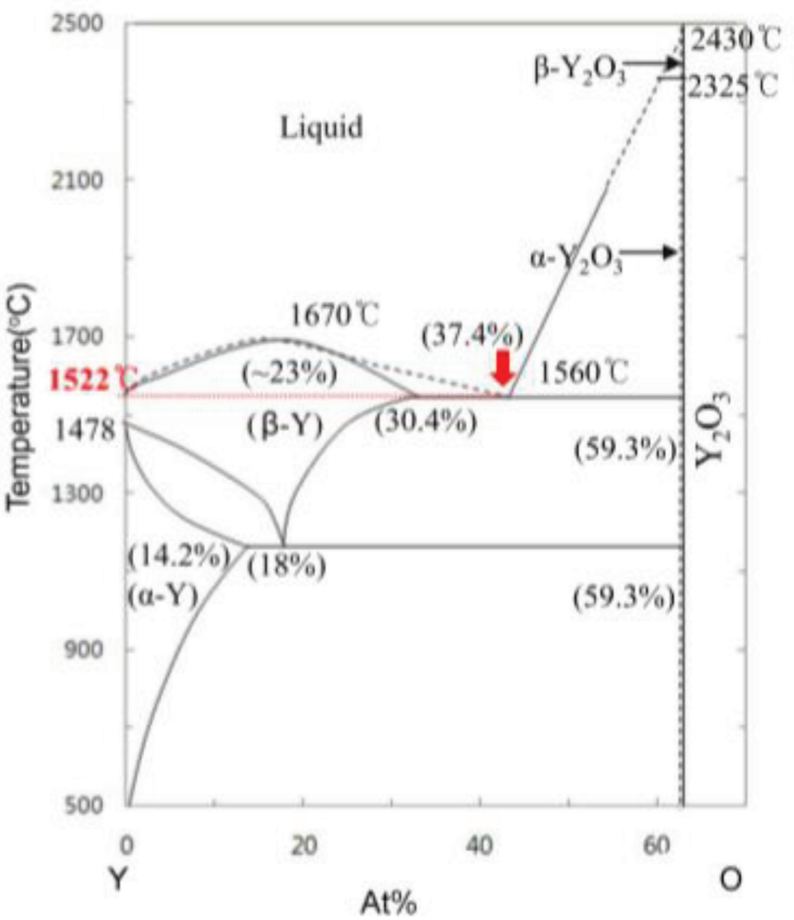

Figure 7.
Phase diagram of yttrium-oxygen [6].

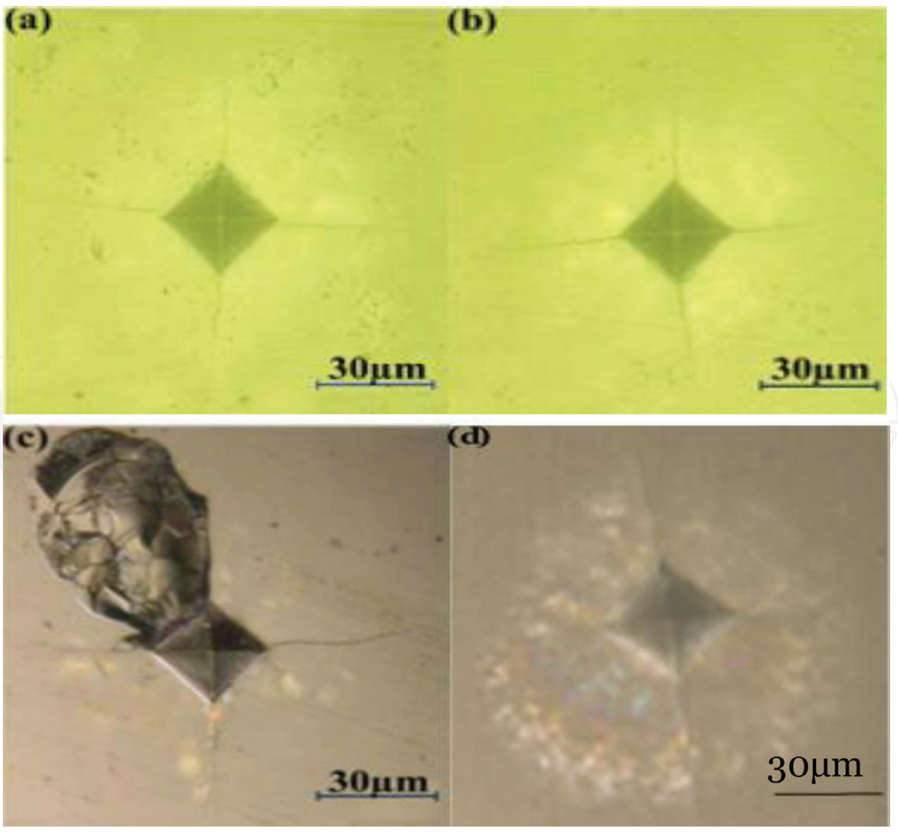

Figure 8.
Vickers indents in sintered polycrystalline yttria ceramics of varying sinter method at 500 g load. Note the general tendency for both more cracking and greater complexity of cracking, particularly near the indent: (a) ASY, as-received yttria; (b) CY, calcined yttria; (c) HY, hot-pressed yttria [17]; and (d) FY, fused yttria.

Name	Grain size (μm)	Young's modulus (GPa)	K_{IC} (GPa)
ASY	<2	146	3.27 ± 0.6
CY	1	153	2.28 ± 0.5
FY	0.8	—	—
HY [17]	>5	168	1.2 ± 0.5

Table 2.
Hardness, Young's modulus, and K_{IC} of yttria ceramics sintered.

and

$$\text{weight loss rate (g/min cm}^2\text{)} = \text{weigh variation (g)/exposure area (cm}^2\text{)} \times \text{exposure time (min)} \times \text{weight before exposure (g)} \quad (3)$$

Quartz and Si wafer (100) were etched at a depth of 2.94–3.14 μm within 10 min of plasma irradiation, and then the etching evaluation was completed. On the other hand, the etching depth of Al_2O_3 and ZrO_2 irradiated with plasma for 60 min was 1.31–1.45 μm. The resistivity of the yttria was 0.41–0.54 μm, which was three times higher than that of the control.

The etching depth and etch rate of the control and yttria specimens was in the order of Si wafer, quartz, ZrO_2, Al_2O_3, and Y_2O_3, as shown in **Figure 10(a)**. The weight loss rate of Al_2O_3 and ZrO_2 was 12 times higher than that of Y_2O_3, as shown in **Figure 10(b)**. In the present study, there was no difference in plasma resistance between the specimens according to the starting materials.

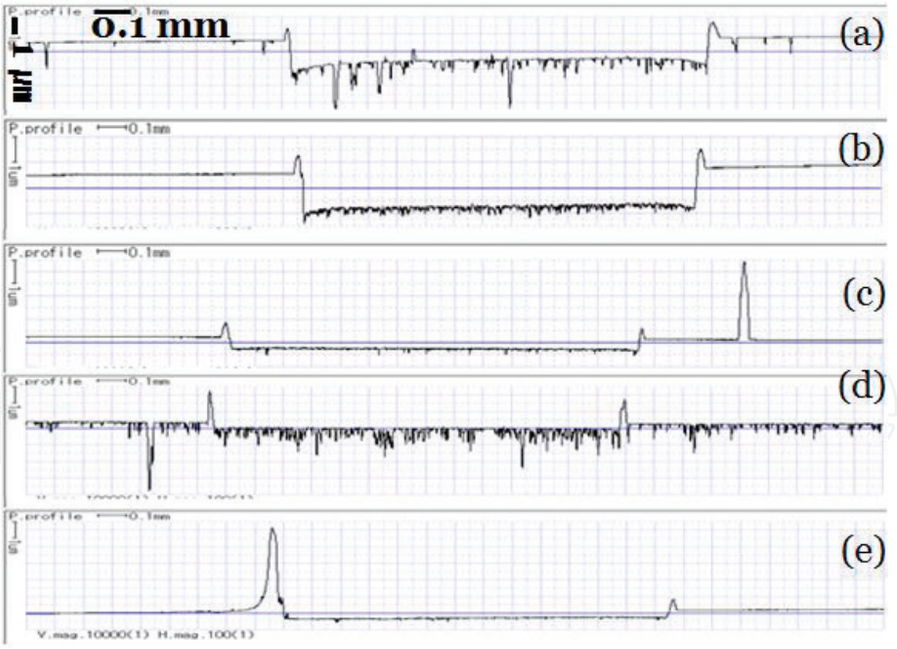

Figure 9.
Coverage of the etching profile for the topographies of the different samples by a plasma test: (a) Al_2O_3, (b) ZrO_2, (c) CY, (d) FY, and (e) HY [17].

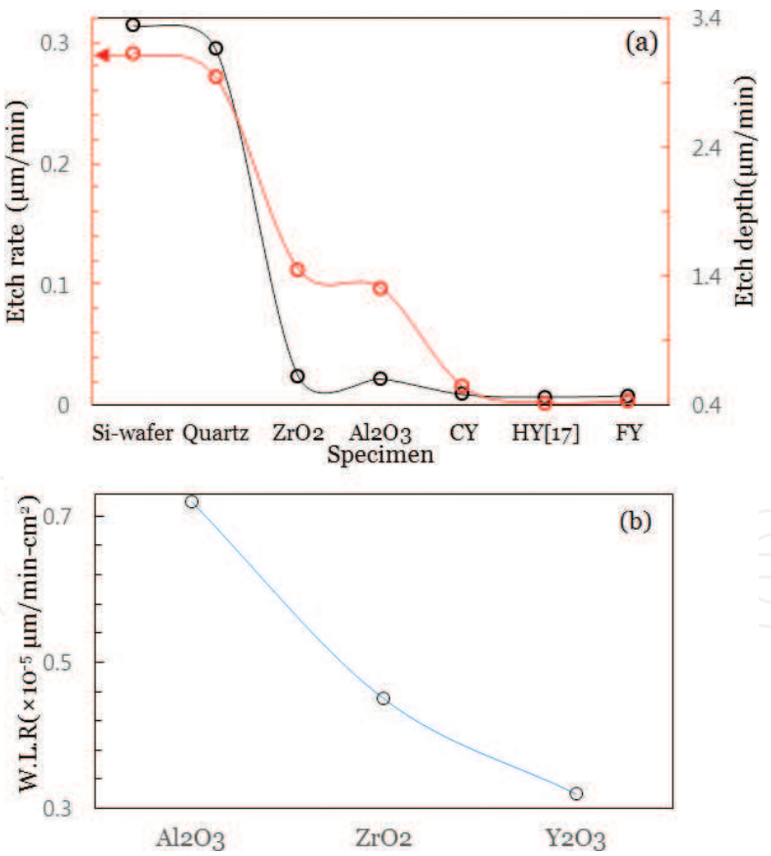

Figure 10.
Coverage of the plasma-deposited yttria ceramics versus quartz, silicon, Al_2O_3, and ZrO_2. (a) Etch depth and rate and (b) weight loss rate and relative weight loss rate. Deposition time of Si wafer (100) and quartz: 10 min. ZrO_2, Al_2O_3, and yttria (CY and HY [17]): 60 min. W. L. R. means the weight loss rate.

1.5 Summary

The plasma resistance and characteristics of the yttria ceramics were investigated in terms of calcination and three-step sintering. The crystal phase of the

calcined yttria ceramics was identified as Y_2O_3, but as-received yttria ceramics contained both Y_2O_3 and $YO_{1.335}$ phase on the XRD pattern have been demonstrated.

The coarse particles in the initial stage changed to uniform particles after repeat-cycle sintering of yttria in air. In the repeated heat treatment process, the liquid phase with local differences in the Y:O ratio was converted to a uniform crystal grain.

The stress propagation along the cleavage plane and the low-level mist shape appeared to the hot-pressed specimen. The Young's modulus increased with decreasing particle size, and K_{IC} appeared to be relatively high regardless of the particle size because the dense microstructure, crystal phase, and the amorphous phase were mixed. The etching depth and etch rate of the control and yttria specimens were in the order of Si wafer, quartz, ZrO_2, Al_2O_3, and Y_2O_3. The weight loss rate of Al_2O_3 and ZrO_2 was 12 times higher than that of yttria ceramics. There was no difference in plasma resistance between the specimens according to the starting materials. The calcination and three-repeated cycle could be suggested as one of effective sintering methods of yttria.

2. Characteristics of thermal oxidation on hot-pressed pure yttria ceramics

2.1 Introduction

Fundamental studies on the forming process that affects the sintering behavior of yttria ceramics and powder synthesis techniques to obtain full density have attracted considerable interest. In particular, the sintering temperature has direct effects on the porosity, density, microstructure or crystal phase, and grain boundary migration. Yttria is used widely as a liquid sintering additive in AlN, SiC, SiAlON, and ZrO_2 [7, 12]. Yttria itself, however, is a sintering-limit material when heated and can induce abnormal grain growth during the sintering process [6].

Finely divided yttria, having a purity at least 99.9%, was pressed into compacts, sintered in a dry hydrogen atmosphere or a partial vacuum to 2150–2300°C, and refired in wet hydrogen at 1950–2300°C to redoxidize any yttria that had been reduced to yttrium during sintering [8]. The resulting polycrystalline yttria ceramics were examined to determine if there was any improvement in the intrinsic properties of yttria.

The previously studied yttria ceramics were divided into three groups. The first was developed from the control of yttria particles, such as 5 nm Y_2O_3 synthesized from a 50 to 120 nm Y_2O_3 powder and $Y(OH)_3$ using a coprecipitation method [9, 24]. The second group was a transparent yttria ceramic used as an infrared window to examine the electrical properties of yttria ceramics with additives, Th, Nd, and Er [15, 28, 29]. The last group involved the development of unconventional sintering techniques, such as triaxial isostatic press, hot isostatic pressing, or vacuum sintering, to fabricate full-density polycrystalline yttria ceramics [13, 30].

Most studies reported that the synthesis of nano-yttria particles was dependent only on the process variables. On the other hand, derivation of a common denominator for the properties of yttria is more complex because of the sintering methods of yttria ceramics, sintering property, and grain boundary migration by dopants such as La, Sr, and Sc [25, 31].

Nevertheless, the purity of the starting material and packing behavior as a function of the particle size used in the granule preparation together with the particle surface area affects the sintering characteristics [13]. These are important factors in the synthesis of dense sintered bodies. When yttria powders are induced on the nanoscale and have high purity, the fine particles or submicron-sized

secondary particles agglomerate easily. Although deformation occurs in most agglomerated particles under applied stresses, strongly agglomerated secondary particles maintain their agglomerated shapes. Because the green compact containing secondary agglomerated particles produces discontinuous microstructures at the interface of the agglomerated zones to show a difference in heat transfer, its evasion is desirable.

From this point of view, a high-purity 99.9% Y_2O_3 powder as a starting material and a hot isostatic pressing method (hot-pressed), which are useful for obtaining a fully dense ceramic, were used to observe the sintering behavior as a function of temperature.

A foundation study was performed through comparisons between the microstructure of hot-pressed yttria ceramics as a function of temperature and that of the density, crystal phase, weight loss, Vickers hardness, the behavior of indentation, flexural strength, etc.

2.2 Characteristics of the hot-pressed yttria ceramics

Figure 11 shows the X-ray diffraction (XRD) patterns of hot-pressed yttria ceramics as a function of temperature. The sintering temperature in hot isostatic pressing (FRET-18, Fuji Denfa, Japan) was increased from 1300 to 1800°C at 100°C intervals, where the heating rate, holding time, and Ar gas flow were 5°C/min, 8 h, and 3 kgf/cm^2, respectively.

The hot isostatic pressing (hot-pressed) yttria ceramic specimens were oxidized at 1200°C for 12 h. XRD revealed the characteristic peaks of cubic yttria (JCPDS 41-1105), as shown in **Figure 11(a)** and **(b)**, irrespective of the sintering temperature and oxidation reaction at 1200°C.

In previous studies using a conventional sintering method, the crystallite phase of yttria could not be described precisely as the yttria phase because the $YO_{1.401}$ (JCPDS39-1064) and $YO_{1.335}$ (JCPDS 39-10,654) phases were also detected in the XRD pattern [25, 31]. This was based on the possibility that lattice distortion due to cation invasion into the oxygen vacancies or the Y-O ions can escape the regular lattice [32]. On the other hand, yttria ceramics containing Sc, Gd, La, Yb, and Mg were accompanied by a change in translucency and grain boundary migration, but the crystal phase was not changed [5].

The change in the intensity ratio reversed the peak at 48 and 57° in the high-temperature region, 1800°C, as shown in **Figure 11(b)**. Therefore, it was necessary to further examine the fraction of the crystal lattice due to the decomposition and volatilization of the yttria component [19, 31]. This means that the yttria crystalline phase varied according to the synthesis conditions and sintering methods, but the Y_2O_3 crystal phase identified in hot-pressed yttria ceramics means that the sintering temperature and oxidation reaction had no effect [18, 33].

Figure 12 shows the hot-pressed yttria ceramics sintered as a function of temperature. As the sintering temperature was increased, the color of the sintered body changed to black. This is dependent on the weight deviation and change in color due to an increase in oxygen defect concentration and Y:O ratio variation [12, 18]. This suggests that the black samples obtained from a traditional sintering method are due to the oxygen released in the lattice site during the sintering process.

In addition, the proposed hot-pressed yttria ceramics could be applied to marking samples with a crystalline structure and full density, because it has a larger effect on the color change than repeat-cycle sintering or conventional sintering. The oxidation reaction specimens were converted to white regardless of the sintering temperature, which suggests that oxygen diffusion affects the

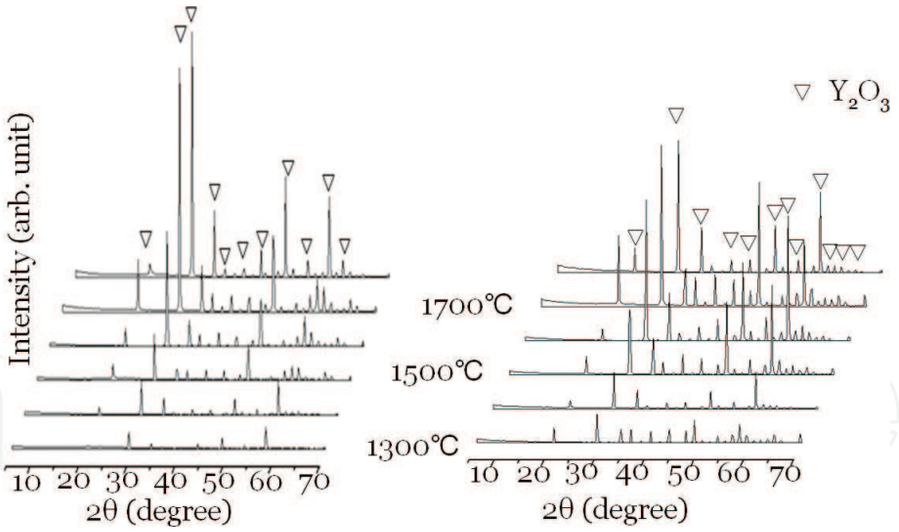

Figure 11.
XRD patterns of yttria ceramic. (a) Hot-pressed yttria ceramics as a function of temperature and (b) tempered in an oxidation of the hot-pressed yttria ceramics at 1200°C in air for 8 h.

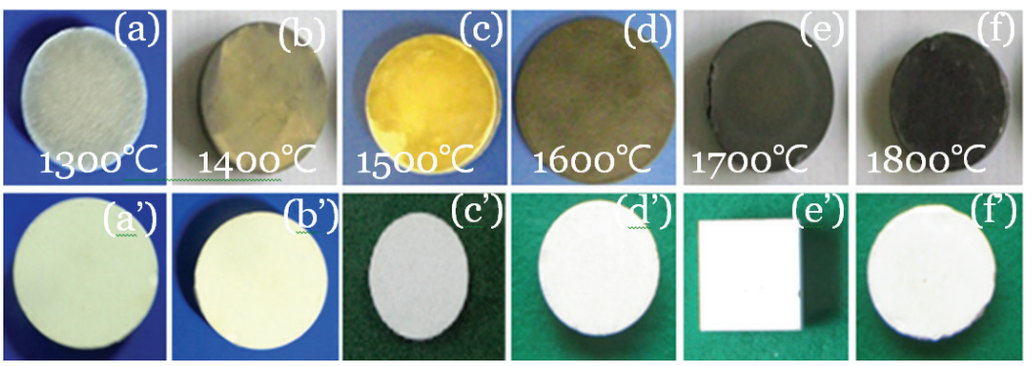

Figure 12.
Colors of yttria samples sintered. (a)~(f) Hot-pressed yttria ceramics as a function of temperature and (a')~(f') tempered in an oxidation of the hot-pressed yttria ceramics at 1200°C in air for 8 h.

oxygen vacancies in the lattice directly [21]. The 1500°C specimen was translucent and showed the considerable development of a glassy phase with increasing sintering temperature.

The weight of the specimens after the oxidation of yttria ceramics showed a tendency to increase with increasing temperature in **Figure 13**. The self-diffusion coefficient of yttrium, D_o, and activation energy, Q, for polycrystalline Y_2O_4 with a density of 99.9% at 1400–1700°C were reported to be 1.65×10^{-2} cm^2/s and 289 J/mole, respectively [31]. The D_o and Q values in the interstitial mechanism at 1050–1250°C were $>6 \times 10^{-6}$ cm^2/s and 82 kJ/mole, respectively [29]. The self-diffusion coefficient was expressed as $D = Do \exp(-Q/RT)$. O had 3.5 times the activation energy of Y, and the self-diffusion of oxygen ions was relatively higher than yttrium. In addition, the diffusion of oxygen anions means that they occur relatively quickly because the interstitial diffusion of yttrium cations was similar to the rate of grain boundary migration [5, 18, 21]. Therefore, the diffusion rate during the oxidation of the hot-pressed yttria ceramics was higher than that of Y atom, and the oxygen vacancy showed preferential filling. This suggests that the weight increases with increasing weight of oxygen (see **Figure 14**).

This tendency corresponded to an approximate 35% reduction in weight due to gas evolution and volatilization in the precursor at temperatures up to 1250°C [10]. The density of the hot-pressed yttria ceramics of 1600°C was close to those of the theoretical density of yttria, 5.03 g/cm^3, and the density tended to decrease

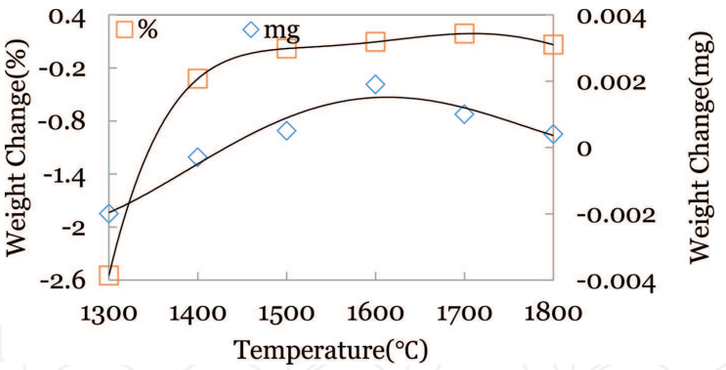

Figure 13.
Behavior of weight of hot-pressed yttria ceramics after oxidation at 1200°C for 12 h in air.

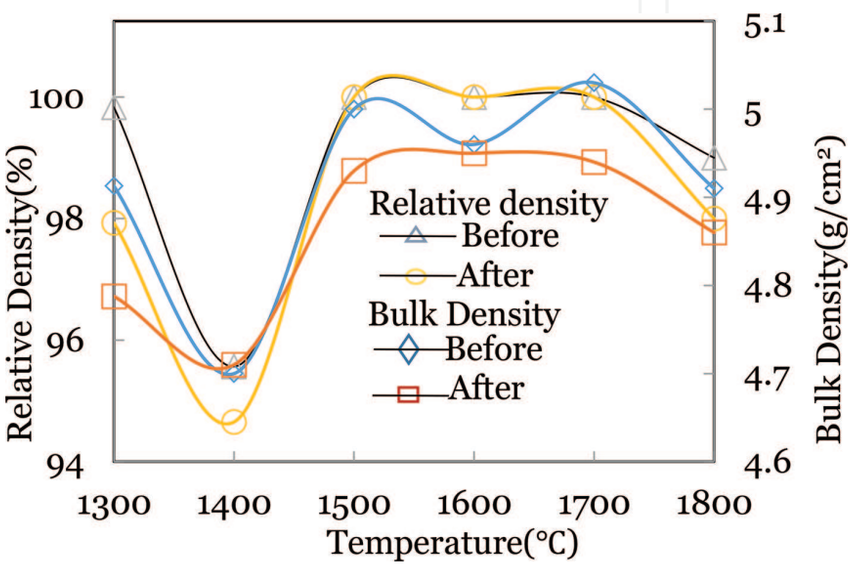

Figure 14.
Bulk and full density of hot-pressed yttria ceramics.

with increasing temperature. **Figure 15** presents SEM images of the microstructure according to the sintering temperature.

The initial 0.5 μm uniform crystal grains changed to a glassy phase, in which the grain size was unclear depending on the sintering temperature, as shown in **Figure 15(a)–(d)**. **Figure 15(e)** and **(f)** presents the grain shape of the pentagonal or hexagonal of 15 μm grain size in yttria ceramics hot pressed at 1700°C. Grain growth tended to show a continuous increase with increasing temperature, which has a direct effect on the porosity, density, and crystal phase (see **Figure 15(a′)–(f′)**). On the other hand, the microstructure of hot-pressed yttria ceramics had an obscurity grain boundary like a glassy phase after the sintering process, which was illustrated by the change in density and weight from **Figure 15(e′)** and **(f)**. The Young's modulus of 120–170 GPa measured by the pulse echo method using an oscilloscope with X and Y modulation in **Figure 16** is believed to be dependent on the yttria ceramic microstructure. **Figure 17** shows the behavior of Vickers indentation of the specimen sintered as a function of temperature.

The indentation shape of the 1400°C specimen showed slightly ragged edges and interior surface, whereas in the 1500°C specimen, the origin, mirror, and mist-like noncrystalline fracture surface were distinguished clearly. The relationship between the grain size and crystal phase was examined by measuring the shape and length of the indentation according to the sintering temperature. This tendency increased with increasing indentation crack length when the crystal

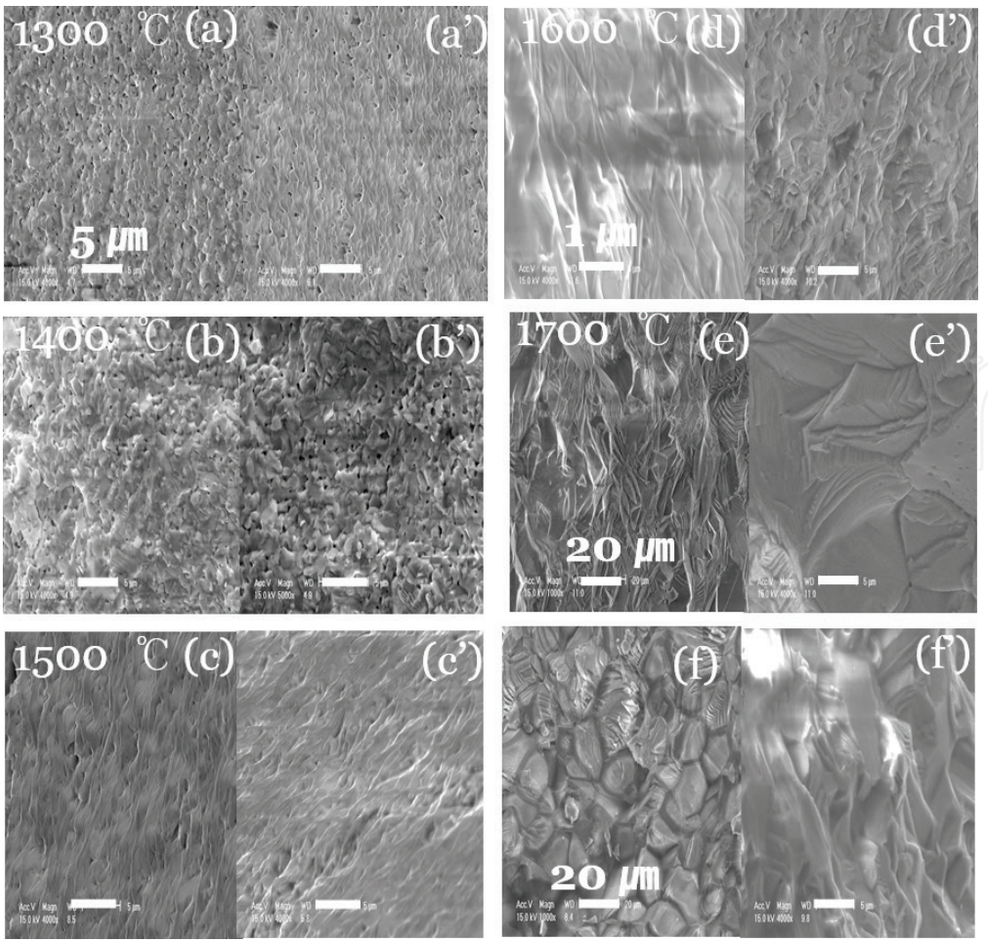

Figure 15.
SEM images of yttria sintered by hot pressing as a function of temperature. (a)~(f) Hot-pressed and (a')~(f') oxidized at 1200°C for 8 h in air.

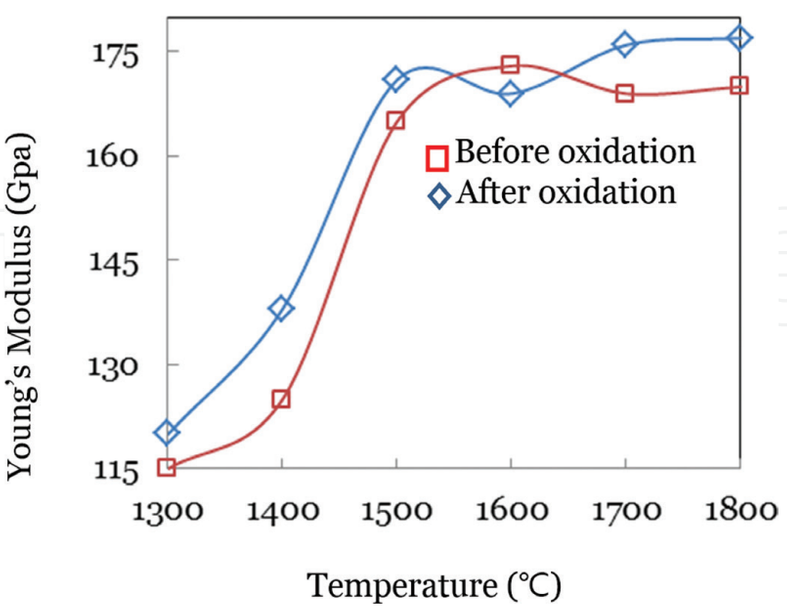

Figure 16.
Young's modulus of yttria ceramic hot-pressed as a function of temperature.

grains of the $MgAl_2O_4$ ceramics were grown from 0.4 to 24 μm and were attributed to the presence of local cracks acting as grain spalling [26]. **Figure 18** shows the K_{IC} and Vickers hardness measured by applying a load of 500 g according to JIS R1610 method. K_{IC} was calculated to be 1.2–1.9 MPa. The displacement point

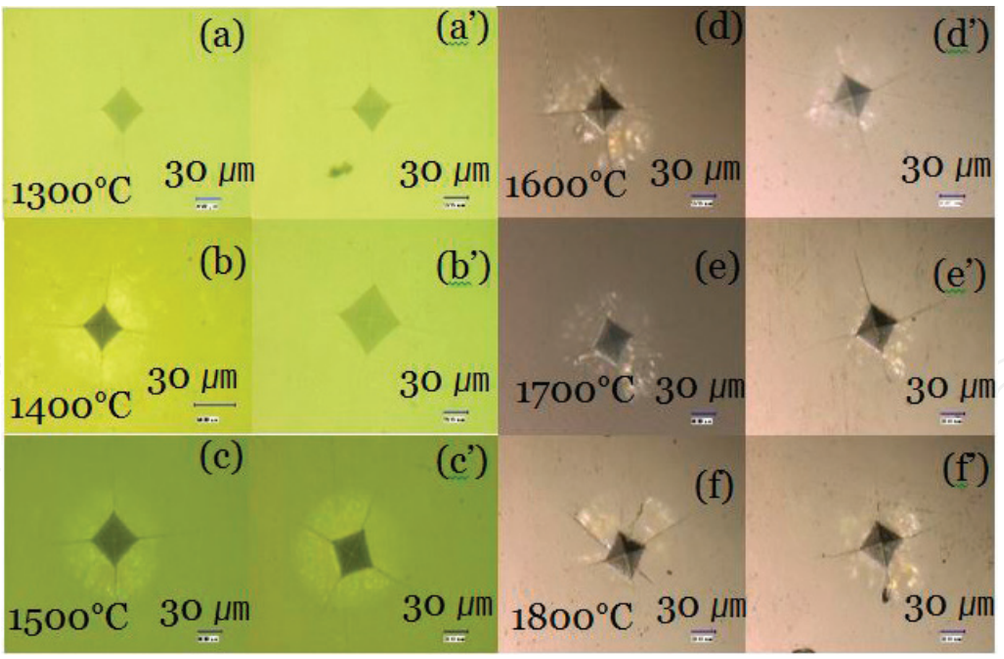

Figure 17.
Indentation images of hot-pressed yttria ceramics; (a)~(f) hot-pressed yttria ceramics as a function of temperature and (a')~(f') tempered in an oxidation of the hot-pressed yttria ceramics at 1200°C in air for 8 h.

of K_{IC} is dependent on the crystal phase according to the sintering temperature. The Vickers hardness of hot-pressed yttria ceramics was 28 GPa, indicating similar properties to those of the conventional polycrystalline yttria ceramics in **Figure 18(b)** [24].

The Vickers hardness of the hot-pressed yttria ceramics had high hardness because the particle size was smaller due to the Hall-Petch effect, but the hardness behavior tended to decrease with increasing particle size [27, 34]. The correlation between K_{IC} and the hardness in hot-pressed yttria ceramics was affected by the

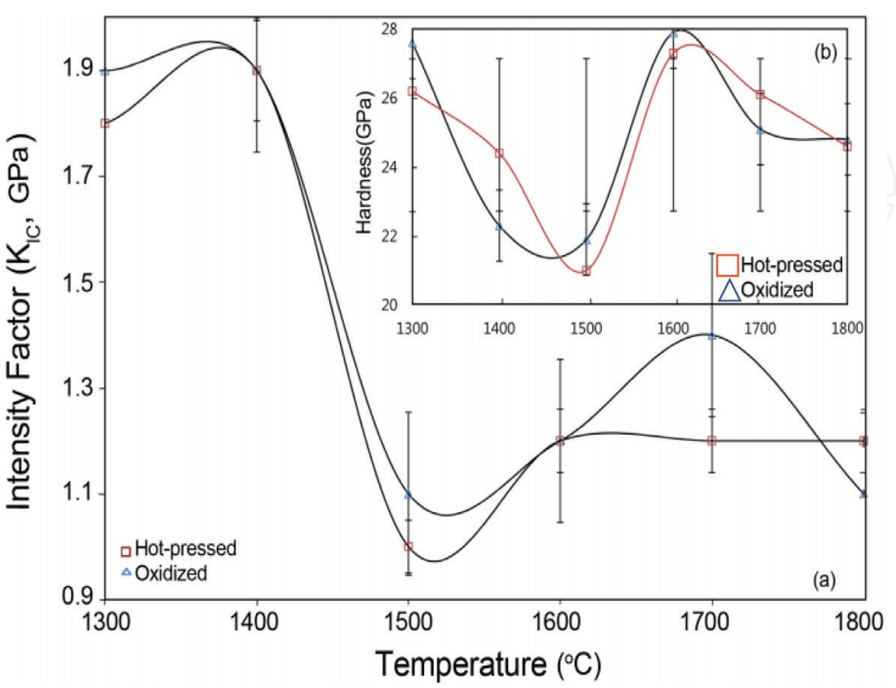

Figure 18.
Hardness and K_{IC} of hot-pressed yttria ceramic. (a) K_{IC} and (b) hardness, 500 g loads, giving typical Vickers indent diagonals. The vertical bars are the standard deviations.

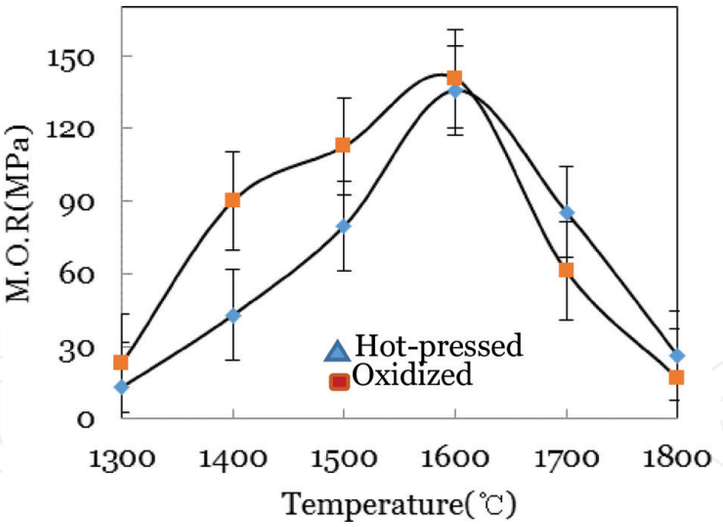

Figure 19.
Flexural strength of hot-pressed yttria ceramics.

grain size and the presence or absence of pores. The mean bending strength of five samples for each specimen was determined according to the JIS R1601 method. **Figure 19** shows the bending strength of the specimen. The specimens before heat treatment showed high strength in the high-temperature region, and those after heat treatment showed relatively high strength in the low-temperature region. The bending strength of the hot-pressed yttria ceramics was approximately 140 MPa, and it was similar to that of fused silica in **Table 3**.

Materials	Fracture toughness (MPa$\sqrt{m}$)	Strength (MPa)
Zirconia (3 mol% Y_2O_3)	7.0–12.0	800–1500
Silicon carbide		
Hot-pressed	4.8–6.0	230–825
Sintered	14.8	96–520
Silicon nitride		
Hot-pressed	4.1–6.0	700–1000
Reaction bonded	3.6	250–345
Sintered	5.3	414–650
Alumina oxide		
99.9% pure	4.2–5.9	282–551
96%	3.85–3.95	358
Hot-pressed yttria	1.0–1.9	20–140
Glass ceramics (Pyroceram)	1.6–2.1	123–370
Fused silica	0.79	104
Borosilicate glass (Pyrex)	0.77	69
Soda-lime glass	0.75	69
Polyethylene terephthalate (PET)	5.0	59.3
Polypropylene (PP)	3.0–4.5	31.0–37.2

Source: ASTM Handbooks, Vol. 1 and 19, Engineered Materials Handbook, Vol. 2 and 4, and Advances Materials & Processes, Vol. 137, No. 6 ASM International Materials Park, OH.

Table 3.
Fracture toughness and strength of various materials.

2.3 Summary

This study examined the characteristics of hot-pressed pure yttria ceramic that was annealed in an oxidation atmosphere. As the sintering temperature was increased, the color of the sintered body changed to black. The weight of the specimens after the oxidation of yttria ceramics showed a tendency to increase with increasing temperature. The hot-pressed yttria ceramics could be applied to marking samples with a crystalline structure and full density. Grain growth tended to show a continuous increase with increasing temperature, which has a direct effect on the porosity, density, and crystal phase. The relationship between the grain size and crystal phase increased with increasing indentation crack length and was attributed to the presence of local cracks acting as grain spalling. K_{IC} was calculated to be 1.2–1.9 MPa, and the Vickers hardness of hot-pressed yttria ceramics was 28 GPa. The specimens before heat treatment showed high strength in the high-temperature region, and those after heat treatment showed relatively high strength in the low-temperature region. The bending strength of the hot-pressed yttria ceramics was approximately 140 MPa. The yttria crystalline phase varied according to the synthesis conditions and sintering methods, but the Y_2O_3 crystal phase identified in hot-pressed yttria ceramics means that the sintering temperature and oxidation reaction had no effect.

Author details

Jin Sam Choi
School of Materials and Engineering, University of Ulsan, Ulsan, R.O. Korea

*Address all correspondence to: jinsamchoi03@gmail.com

References

[1] Hönninger C, Zhang G, Keller U, Giesen A. Femtosecond Yb-YAG laser using semiconductor saturable absorbers. Optics Letters. 1995;**20**(23):2402-2024

[2] Takaichi K, Yagi H, Lu J, Shirakawa A, Ueda K, Yanagitani T, et al. Yb^{3+}-doped $Y_3Al_5O_{12}$ ceramics—A new solid-state laser material. Physica Status Solidi. 2003;**200**(1):5-7

[3] Kodo M, Soga K, Yoshida H, Yamamoto T. Low temperature sintering of polycrystalline yttria by transition metal ion doping. Journal of the Ceramic Society of Japan. 2009;**117**(6):765-768

[4] Harris DC. Materials for Infrared Windows and Domes. Washington, USA: SPIE-The International Society for Optical Engineering; 1999

[5] Lapato LM, Shevchenko AV, Kushchevskii AE. Polymorphic transitions of rare earth oxides at high temperatures. Inorganic Materials. 1974;**10**(8):1276-1281

[6] Carlsson ON. The O-Y (oxygen-yttrium) system. Bulletin of Alloy Phase Diagrams. 1990;**11**(1):61-66

[7] Iwasawa J, Nishimizu R, Tokita M, Kiyohara M, Uematsu K. Plasma resistance dense yttrium oxide film prepared by aerosol deposition process. Journal of the American Ceramic Society. 2007;**90**(8): 2327-2332

[8] Muta A, Tsukuda Y. Method for Sintering Very Pure Yttria Compacts to Transparency. U.S. Pat. 3,764,643; 1973

[9] Chen IW, Wang XH. Sintering dense nanocrystalline ceramics without final-stage grain growth. Nature. 2000;**404**:168-171

[10] Saito N, Matsusa SI, Ikegami T. Fabrication of transparent yttria ceramics at low temperature using carbonate-derived powder. Journal of the American Ceramic Society. 1998;**81**(8):2023-2028

[11] Chen PL, Chen IW. Grain boundary mobility in Y_2O_3: Defect mechanism and dopant effects. Journal of the American Ceramic Society. 1996;**79**(7): 1801-1809

[12] Jorgensen PJ, Anderson RC. Grain-boundary segregation and final stage sintering of Y_2O_3. Journal of the American Ceramic Society. 1967;**50**(11):553-558

[13] Huang Y, Jiang D, Zhang J, Lin Q. Fabrication of transparent lanthanum-doped yttria ceramics by combination of two-step sintering and vacuum sintering. Journal of the American Ceramic Society. 2009;**92**(12): 2883-2887

[14] Druschitz AP, Schroth JG. Hot isostatic pressing of a presintered yttria-stablized zirconia ceramic. Journal of the American Ceramic Society. 1989;**72**(9):1591-1597

[15] Greskovich C, Woods KN. Fabrication of transparent ThO_2-doped Y_2O_3. Journal of the American Ceramic Society Bulletin. 1973;**52**(5):47378

[16] Katayama K, Osawa H, Akiba T, Yanagida H. Sintering and electrical properties of CaO-doped Y_2O_3. Journal of the European Ceramic Society. 1990;**6**:39-45

[17] Choi JS, Shin DW, Bae WT. Characteristics of thermal oxidation on hot-pressed pure yttria ceramics. Journal of the Korean Ceramic Society. 2013;**50**(3):180-185

[18] Chen PL, Chen IW. The role of defect interaction in boundary mobility and cation diffusivity of CeO_2. Journal of the American Ceramic Society. 1994;**77**(9):2289-2297

[19] Jollet F, Noguera C, Gautier M, Thromat N, Duraud JP. Influence of oxygen vacancies on the electronic structure of yttrium oxide. Journal of the American Ceramic Society. 1991;**74**(2):358-364

[20] Shannon RD. Revised effective ionic radii and systematic studies of interatomic distances in halides and chalcogenides. Acta Crystallographica. 1976;**A32**:751-767

[21] Kingery W, Bowen H, Uhlmann D. Introduction to Ceramics. 2nd ed. New York, U.S.A.: John Wiley & Sons Inc.; 1976. p. 418, 431 and 505

[22] Ikegami T, Li JG, Mori T. Fabrication of transparent yttria ceramics by low temperature synthesis of yttrium hydroxide. Journal of the American Ceramic Society. 2002;**85**(7):1725-1729

[23] Rhodes WH, Trickett EQ, Sordelet DJ. Key powder characteristics in sintered optical ceramics. Ceramic Transactions. 1990;**12**:677-690

[24] Nobby T, Kofstad P. Electrical conductivity and defect structure of Y_2O_3 as a function of water vapor pressure. Journal of the American Ceramic Society. 1984;**67**(12):786-792

[25] Swamy V, Dubrovinskaya NA, Dubrovinsky LS. High-temperature powder X-ray diffraction of yttria to melting point. Journal of Materials Research. 1999;**14**(2):456-459

[26] Rice RW, Carl CW, Borchelt F. Hardness-grain-size relations in ceramics. Journal of the American Ceramic Society. 1994;**77**(110):2539-2553

[27] Armstrong RW, Raymond EL, Vandervoort RR. Anomalous increases in hardness with increase in grain size of beryllia. Journal of the American Ceramic Society. 1970;**53**:529-530

[28] Ikesue A, Kamata K, Yoshida K. Synthesis of transparent Nd-doped HfO_2-Y_2O_3 ceramics using HIP. Journal of the American Ceramic Society. 1996;**79**(2):359-364

[29] Berard MF, Wilder CD. Cation self-diffusion in polycrystalline Y_2O_3 and Er_2O_3. Journal of the American Ceramic Society. 1969;**52**(2):85-88

[30] Choi JS, Bae WT. Full Density Yttria Ceramic Sintered by Using for Conventional Sintering Method with Fused Yttria as Starting Materials. Kr. Pat. No: 10-2012-0082809; 2012

[31] Berard MF, Wirkus CD, Wilder DR. Diffusion of oxygen in selected rare earth oxides. Journal of the American Ceramic Society. 1968;**51**(11):643-647

[32] Ackermann R, Rauh E, Walters R. Thermodynamics study of the system yttrium + yttrium sesquioxide A refinement of the vapor pressure of yttrium. The Journal of Chemical Thermodynamics. 1970;**2**:139-149

[33] Verkerk MJ, Winnubst AJA, Burggraf AJ. Effect of impurities on sintering and conductivity of yttria-stabilized zirconia. Journal of Materials Science. 1982;**7**:3112-3113

[34] Christopher S, Nieh TG. Hardness and abrasion resistance of nano crystalline nickel alloys near the Hall Petch breakdown regime. Materials Research Society Symposium Proceedings. 2003;**740**:27-32